Development of a Molecular Assessment High-Resolution Observation Spectrometer (MAHOS) for Microsatellites

Maho Nakagawa, Takayoshi Yamada, Shigeru Sato, Ichiro Kato, Toshiyuki Nishibori, Kenichi Harada, Toru Taniguchi, Hiroaki Kawamoto, Kazuyuki Nakamura, Takahiro Kuhara, and Yasuko Kasai

***Abstract*—Compact and lightweight sensors with a high-frequency resolution are required for the passive observation of atmospheric water and oxygen emission lines at a reduced cost and power consumption. A molecular assessment high-resolution observation spectrometer (MAHOS) is developed as a compact, low power, digital fast Fourier transform spectrometer to be installed on a microsatellite. MAHOS has a compact design with dimensions of 0.154 × 0.125 × 0.040 m^3 and mass of 0.7 kg. It uses only a few materials including a field-programmable gate array (FPGA) module with a lightweight aluminum alloy box. The highly stable spectrometer exhibits a sampling speed of 2.6624 GS/s and 16 384 frequency channels. The stability of the spectrometer is longer than 1200 s within the 1-GHz bandwidth. Thermal dissipation is achieved through a heat conductive gel filled in the gap between the most heat-generating component, the FPGA, and the aluminum alloy case. Results of a finite element analysis indicate that the design is stiff and stable enough to survive in the launch environment. Thermal analysis indicates the durability of the system during operation. Even in space where heat dissipation is not possible, self-heating temperatures are not a problem for the FPGA. In the future, the performance of the spectrometer will be verified by conducting environmental tests.**

***Index Terms*—Aerospace simulation, Fourier spectroscopy, remote sensing, satellite applications, spectral analysis.**

Manuscript received May 7, 2021; revised June 17, 2021; accepted June 27, 2021. Date of publication June 30, 2021; date of current version March 31, 2022. This work was supported in part by the Research and Development Program on Key Technology in Terahertz Frequency Bands of the Ministry of Internal Affairs and Communications under Grant JPJ000254. *(Corresponding author: Maho Nakagawa.)*

Maho Nakagawa, Takayoshi Yamada, Shigeru Sato, and Ichiro Kato are with the Terahertz Technology Research Center, National Institute of Communication and Technology, Tokyo 184-8795, Japan (e-mail: nakagawa66@nict.go.jp; yamada-takayoshi@nict.go.jp; sato-shigeru@nict.go.jp; ikato@nict.go.jp).

Toshiyuki Nishibori is with the Institute of Space and Astronautical Science, Japan Aerospace Exploration Agency, Tsukuba 305-8505, Japan (e-mail: nishibori.toshiyuki@jaxa.jp).

Kenichi Harada, Toru Taniguchi, and Hiroaki Kawamoto are with Engineering Department Section 1, Applied Elecs Industry Company, Ltd., Kanagawa 213-0014, Japan (e-mail: harada@elecs.co.jp; taniguchi@elecs.co.jp; kawamoto@elecs.co.jp).

Kazuyuki Nakamura and Takahiro Kuhara are with the Engineering Department, Applied Technosolver Corporation, Kanagawa 252-0804, Japan (e-mail: kazuyuki.nakamura@techsol.jp; takahiro.kuhara@techsol.jp).

Yasuko Kasai is with the Terahertz Technology Research Center, National Institute of Communication and Technology, Tokyo 184-8795, Japan, and also with the Physics Program, Graduate School of Pure and Applied Sciences, Tsukuba University, Tsukuba 305-8577, Japan (e-mail: ykasai@nict.go.jp).

Digital Object Identifier 10.1109/JMASS.2021.3093549

I. Introduction

MEASUREMENTS of chemical species in the atmosphere provide accurate information on their formation processes, emission sources in the atmosphere. The water (H_2O) and oxygen (O_2) concentrations can provide detailed information on the forecast of increasingly intense typhoons on Earth and the altitude distribution of the unobserved planetary atmospheric components. In particular, Mars has been suggested by simulations and observation to have H_2O and O_2 [1]–[3]. For example, if we obtain this information from the altitude of the middle atmosphere (about 80–130 km), which is yet unknown from actual measurements, we will learn how the water environment is changing on Mars [4], [5].

The instruments operating in the terahertz (THz) frequency range are feasible for constructing a compact and lightweight, with high-frequency resolution, microsatellite. The THz range is defined as the submillimeter range from 300 to 3000 GHz [6]. Especially, the 0.48-THz (480-GHz) band is a key to installing a compact microsatellite, because the H_2O and O_2 concentrations can be simultaneously observed in this range [1].

To capitalize on the advantage of this frequency band, our group is developing a THz sensing system (THzSens) receiver using heterodyne detection techniques [7]. Because of cheap launching costs, the miniaturization of a THzSens receiver weighing several kilograms can not only be used for satellite constellation system on Earth orbits as launching

series of satellites but also facilitate the accessibility of planetary exploration, because the launch cost can be significantly decreased from a few hundred million Euros to a few million Euros from mounting this receiver on microsatellites weighing in the range of 50 kg. The microsatellite volume and mass requirements are less than one cubic meter and less than 100 kg, respectively [8]. The volume, power consumption, and mass requirements of the payload bus of a THzSens receiver (e.g., [9]) are less than $0.50 \times 0.50 \times 0.50$ m^3, 30 W, and less than 30 kg, respectively. As an optical back-end component of the receiver, this study aims to develop a small, lightweight, and low-power-consuming spectrometer.

To analyze the emission line spectrum of gaseous components of the atmosphere for remote sensing, various spectrometers have been developed for atmospheric remote sensing, of which the three main types are acousto-optic spectrometers (AOSs), chirp transform spectrometers (CTSs), and digital fast Fourier transform (FFT) spectrometers [10]. The AOSs using the diffraction effect of laser light are used on the superconducting submillimeter-wave limb-emission sounder (SMILES) and the submillimeter-wave astronomy satellite (SWAS). It is noted that the SWAS on the Odin satellite remains in Earth orbit, but is in standby and not operational. The AOS employed in SMILES, which operates at 625–650 GHz onboard the international space station, has the following specifications: volume of 0.027 m^3, mass of less than 13.6 kg, and power consumption of 37 W [11]. The AOS employed in SWAS, which operated in spectral regions at approximately 487, 492, 548, 551, and 557 GHz on the Odin satellite, had a mass of 7.5 kg and power consumption of 5.5 W with full operation [12], [13]. These AOSs needed to be installed on a large payload bus, and could not be mounted on a microsatellite. In contrast, a CTS, utilizing a chirp filter to the spectrum using chirp waveforms in pulse-compression radar, is developed for the submillimeter wave instrument (SWI) of the ESA microsatellite Jupiter ICy moons Explorer [14]–[16]. It is integrated into several trays containing other individual electronics subsystems as a component of the electronic unit and provides 1-GHz bandwidth at 100-kHz resolution. However, the unit, including the CTS, is designed to be mounted on a large satellite, and the power consumption of the SWI is less than 50-W power [17]. Recently, a digital FFT comprising a fast analog-to-digital converter (ADC) and field-programmable gate array (FPGA) circuits in real time has been developed for radio astronomical sensing and atmospheric remote sensing [18]. Digital FFT spectrometers exhibit the following advantages: they do not require the temperature stability required by AOSs, facilitate longer stability without calibration, and are much cheaper [19]. The fast Fourier transform spectrometers (FFTS) for the Atacama pathfinder experiment (APEX) telescope was developed for radio astronomical sensing as high-resolution broadband spectrometers in the Max-Planck-Institute für Radioastronomie [20]. The FFTS has the following specifications: volume of 0.031 m^3, and 13 kg, and are assumed for ground use [21]. However, it has potential for mounting on spacecrafts and satellites because of the thin FFTS-board (0.016 m^2) and the power consumption of less than 20 W [22]. In fact, a modified version of the FFTS, the extended bandwidth, XFFTS, has been employed on a German receiver for astronomy at terahertz frequencies (GREAT) operated in the stratospheric observatory for infrared astronomy (SOFIA) for the astronomical observation [23]. The size and power consumption are almost the same as commercial products, 2.5 GHz with 32 k spectral channel and consumes 20–25 W, but with a spectral resolution of 88.5 kHz.

The FFT technology is also using atmospheric remote sensing. For example, a compact spectrometer of volume 1.2×10^{-4} m^3 and mass 0.119 kg on PCB in a custom casing, with peak power consumption as low as 0.65 W for the entire system, has been developed [24]. For example, this circuit board was used in the compact adaptable microwave limb sounder (CAMLS), which has 0.01 m^3 volume, approximately 10-kg weight, and 70-W power consumption, at 340 GHz [25]. This sounder aims to observe the composition, humidity, temperature, and clouds in Earth's upper troposphere and stratosphere. However, its resolution is not very high; thus, it is not suitable for observing the fine structure of emission lines in the atmosphere. Our proposed receiver targets to mainly observe H_2O and O_2 concentrations. Hydrogen peroxide and a single ozone absorption line are also in the observation range, although the signal is very small compared to water and oxygen [1]. A high resolution also would allow us to obtain this information at 1-GHz bandwidth.

Therefore, it is important to design and manufacture a new compact and high-resolution spectrometer that can be mounted on small satellites. Accordingly, we have developed a compact FFT spectrometer, called a molecular assessment high-resolution observation spectrometer (MAHOS), with the required volume, mass, and power consumption of approximately $0.150 \times 0.120 \times 0.040$ m^3 with each margin of less than 0.005 m, less than 1.0 kg, and at least 5 W, respectively. We plan to install this spectrometer on microsatellites or CubeSat, it is essential to reduce its volume and weight. Although digital spectrometers are disadvantageous in terms of power consumption, the recently developed digital FFT has achieved low-power consumption. To the best of our knowledge, there have not been so far any previous developments of the spectrometer with a small-size, lightweight, and power-saving design with a sufficiently high-frequency resolution for satellites. MAHOS is a simple configuration of a mechanically superior package and has a volume of approximately one-fourteenth that of CAMLS.

As described below, MAHOS for microsatellites was realized by parts downsizing and many technics especially around the FPGA, ADC, etc. This article presents the MAHOS design and validates its application as a space-use system through electrical performance evaluation tests and thermal and structural analyses. The remainder of this article is organized as follows. Sections II and III present the system architecture and mechanical design of MAHOS with the THzSens receiver, respectively. Section IV discusses the measuring system's electrical performance. Section V evaluates the structural analysis and thermal stress for the MAHOS system. Section VI concludes this article.

TABLE I
MAHOS SPECIFICATIONS FOR THE RECEIVER

Items		Requirements	Specifications
Volume (m^3)		0.150 × 0.120 × 0.040 margin ±0.005	0.154 × 0.125 × 0.040
Mass (kg)		< 1.0	0.70
Operating temperature range (°C)		-15 to +50	-15 to +50
Storage temperature range (°C)		-20 to +60	- 40 to +100
Number of IF inputs		1 ≤	1 or 2 (Depends on operating mode)
Power consumption* (W) * The LO signal is shared with the mixer section and its power consumption is included in the mixer.		Minimum 5	5 (1/6 intermittent×1 ch) 6 (1/3 intermittent×1 ch, 1/6 intermittent×2 ch) 7 (1/2 intermittent×1 ch) 10 (continuous acquisition×1 ch, 1/2 intermittent×2 ch)
Frequency resolution (kHz)	Integration time (s)	1	1
	Frequency range (GHz)	5.5 - 6.5	5.33 – 6.65 (With BPF 5.5 - 6.5)
	Frequency channel		16,384
	Channel separation (kHz)	< 100	81.25
	Sampling frequency (Gsample/s)		2.6624
Dynamic range (dB)		30	30 <
FFT resolution (bit)		-	12
Input power (dBm) / 5.5 - 6.5 GHz		-20 - -26	-23

II. SYSTEM ARCHITECTURE

The spectrometer, MAHO, exhibits a simple measurement system, where the FFT technology is used to cut a continuous input signal into several sampling points (the time-window length) for analysis. In this study, we focus on the 480-GHz region to simultaneously observe the height distributions of H_2O and O_2 in the Earth or planetary atmosphere within the 1-GHz range through passive heterodyne detection. The receiver system can separate upper sideband (USB) and lower sideband (LSB), and the signal fall within the 1-GHz bandwidth with a suitably chosen LO frequency. For example, an absorption line exhibits H_2O at 474.69 GHz and O_2 at 487.25 GHz [1]. In this study, a frequency resolution of less than 100 kHz is set as suggested in [1], because we might observe hydrogen peroxide and ozone absorption lines besides the H_2O and O_2 lines. This spectrometer installed on the THzSens receiver must be highly versatile and able to handle various observation situations. A resolution of less than 100-kHz resolution over a 1-GHz bandwidth is required over 10 000 frequency channels with a sampling speed over 2 GS/s. In our design, MAHOS can perform measurement at 2.6624 GS/s over 16 384 frequency channels with a double-sideband spectrum. These specifications satisfy the required resolution of 81.25 kHz.

In addition, the Hanning or Blackman window function can be selected for encoding and multiplication with the ADC output. Under the application of a time window, which refers to a finite-time length cut from a real signal, the spectrum undergoes significant broadening. The FFT operation is performed by cutting a finite-time length from a real signal and treating it as a repeated waveform. When the time length is an integer multiple of the input signal period, the waveform is continuous and a correct spectrum is obtained. If the resolution is defined as the width of the main lobe, the window function reduces the frequency resolution.

However, the signals at other frequencies can be detected more easily to suppress the side lobes. Without the window function, the main lobe is narrower, whereas the side lobes are larger and the power spectrum leaks into a wider band. Thus, the purpose of the observation decides the application of the functions.

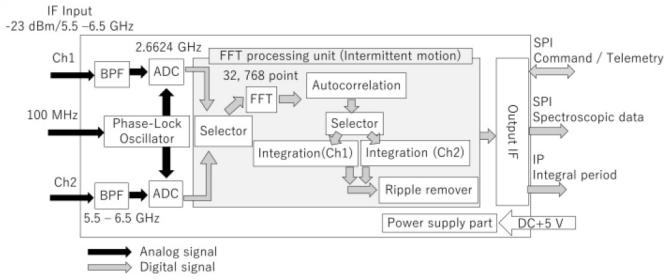

Fig. 1. Redundant mechanical system layout of MAHOS.

Fig. 1 shows a block diagram of the developed MAHOS system. This spectrometer comprises bandpass filters (BPFs), ADCs, and an FFT processing unit, which contains an autocorrelator for converting the FFT output to power spectra, integrated functions, and a ripple remover. After passing through the BPF, the IF output signal becomes 5.5–6.5 GHz and is then digitized by the ADC. The aliasing of other undesired signals is avoided by applying the 5th Nyquist zone of 0–1.33 GHz. Then, the digitized signal is passed through the FFT processing unit, which is controlled by the intermittent motion for power consumption.

In the integration stage, the channels are selected and the autocorrelation function is calculated in real time. After the FFT, the circuit is shared by time multiplexing when these two channels are used simultaneously. Finally, the serial peripheral interface (SPI) signal is through the ripple removing unit and electrical connections to a data handling and power supply unit (DH/PSU) by using an MDM connector. The oven-controlled crystal oscillator provides +5 dBm of 100 MHz clocks as a master clock for the ADC to ensure correct operation.

The function of the system was developed based on the principle of a digital instrument platform, called optically connected transmission system for analog-to-digital conversion (OCTAD-S) [26]. Table I summarizes the specifications of MAHOS. The internal technical system has been designed and

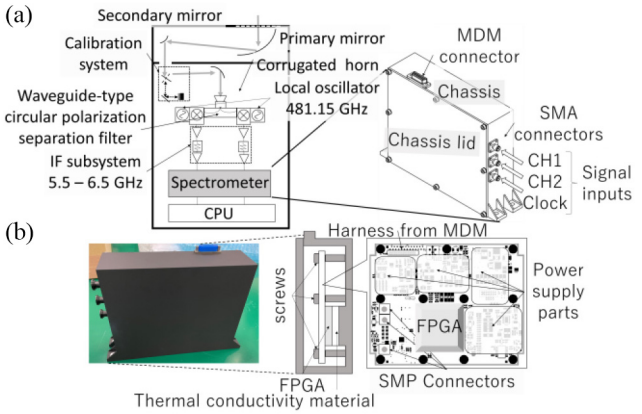

Fig. 2. (a) Overview of the THzSens receiver and external view of MAHOS. (b) Image and internal view of the MAHOS prototype.

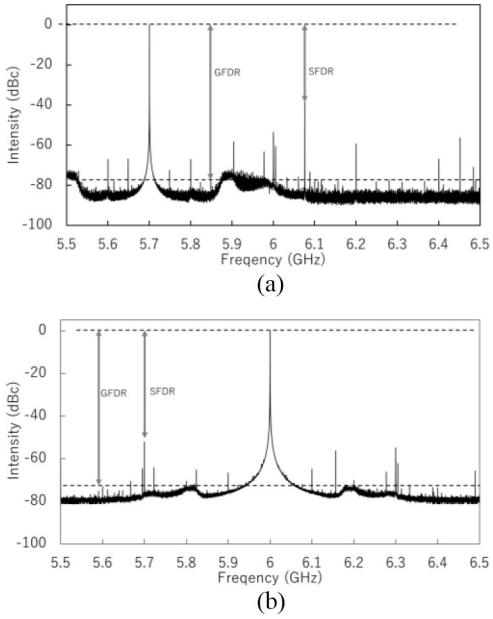

Fig. 3. SFDR and GFDR with 1-GHz bandwidth generated by a signal generator at (a) 5.7 GHz and (b) 6.0 GHz.

manufactured by *Elecs Industry Company, Ltd.,* and essentially comprises an FPGA, a BPF, dc–dc converters, and an ADC on a printed circuit board. FPGA is reprogrammable, which allows for flexibility as the bus section is developed. The operating temperature range in the bus section is maintained within −15 to +50 °C with the normal performance of FPGA, which is the self-heating component. The FPGA is connected to the heat dissipation plate and a heat conductive gel, which is integrated with the aluminum alloy case. The power consumption can be selected from 5 to 10 W by the intermittent operation modes with 1-s integration time per spectrum. As a countermeasure to a single-event latch-up, DH/PSU provides a power on/off control feature for MAHOS. This function aims to protect the device from single-event latch-up and failure by isolating it from the bus power supply.

III. Mechanical Design

This section summarizes the MAHOS design concept and provides a brief overview of the THzSens receiver.

Fig. 2(a) presents a schematic overview of the THzSens receiver and external view of MAHOS for the microsatellite. The volume of the optical bench for the THzSens receiver is approximately 0.384 × 0.384 × 0.360 m^3, with a maximum mass of < 10 kg and total power consumption of less than 30 W. We can observe H_2O and O_2 emission lines in the atmosphere using heterodyne techniques across two frequency bands: 486.64–487.64 GHz (USB) and 475.64–474.64 GHz (LSB). The THz radiation from the atmosphere reaches MAHOS as the end of the backend with passing through mirrors and calibration system unit in the frontend [27]. A phase-locked dielectric 13.365-GHz resonator oscillator and an oven-controlled 100-MHz crystal oscillator clock are used for generating the local oscillator (LO) source, which is amplified to 240 GHz using an integrated amplifier multiplier chain (IAMC). The 480-GHz subharmonic mixer is pumped with sufficient LO power and used to downconvert the radio frequency (RF) of the input signal to an intermediate frequency (IF) of 6 GHz [1]. The input signal was amplified using two amplifiers and digitized using MAHOS. The IF inputs and reference clock input signals are obtained from three SMA connectors. The instrument is synchronized by branching an external 100-MHz reference clock to be used as the LO signal. A micro Dsub metal (MDM) connector for the supplied dc and SPI is mounted on the top.

The chassis is strength-designed and manufactured by *Technosolver Corporation* and *EMTECH Corporation*, respectively. The entire chassis is made of aluminum alloy, whose surface is painted black to create a uniform temperature inside the THzSens field and promote thermal radiation. The chassis is a single piece of machined parts. The chassis with mounting legs has a volume of 0.154 × 0.125 × 0.040 m^3 and is fixed on the floor with four screws [Fig. 2(b)]. Table II lists the mass allocation of the following subcomponents: 1) key components, such as FPGA, BPF, dc–dc converters, and ADC, including the coating material and glue; 2) chassis and mounts; and 3) accessories, such as bolts, nuts, SMA connectors, and harness.

IV. Methods and Procedures

A. System Performance

This section demonstrates the performance of MAHOS with respect to frequency stability, signal sensitivity, input response, and Allan variance through laboratory experiments.

The frequency response with 1-GHz bandwidth is measured by an input signal generator at 5.7 and 6.0 GHz (Fig. 3).

These input signals are displayed with harmonics and some large and small spurious signals. The harmonics and large spurious, so-called spurious-free dynamic range (SFDR), refers to the frequency components above the floor level and less than the input signal that appears in the output signal despite the presence of the input signal. As compared to the result obtained at 6 GHz, the harmonic components of the input signal overlap with the spurious components, which can significantly deteriorate the SFDR, especially at 5.7 GHz, which

TABLE II
MASS ALLOCATION OF THE SUBCOMPONENTS

Items		Requirements	Specifications
Volume (m^3)		0.150 × 0.120 × 0.040 margin ±0.005	0.154 × 0.125 × 0.040
Mass (kg)		< 1.0	0.70
Operating temperature range (°C)		-15 to +50	-15 to +50
Storage temperature range (°C)		-20 to +60	- 40 to +100
Number of IF inputs		1 ≤	1 or 2 (Depends on operating mode)
Power consumption* (W) * The LO signal is shared with the mixer section and its power consumption is included in the mixer.		Minimum 5	5 (1/6 intermittent×1 ch) 6 (1/3 intermittent×1 ch, 1/6 intermittent×2 ch) 7 (1/2 intermittent×1 ch) 10 (continuous acquisition×1 ch, 1/2 intermittent×2 ch)
Frequency resolution (kHz)	Integration time (s)	1	1
	Frequency range (GHz)	5.5 - 6.5	5.33 – 6.65 (With BPF 5.5 - 6.5)
	Frequency channel		16,384
	Channel separation (kHz)	< 100	81.25
	Sampling frequency (Gsample/s)		2.6624
Dynamic range (dB)		30	30 <
FFT resolution (bit)		-	12
Input power (dBm) / 5.5 - 6.5 GHz		-20 - -26	-23

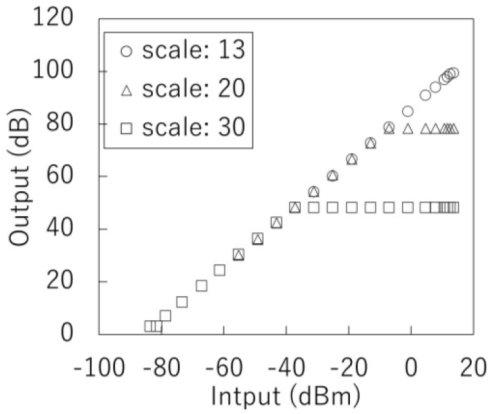

Fig. 4. Response of the input generated by a signal generator at 5.9 GHz. These scales can measure each input signal range.

overlaps with the 6.07-GHz signal under the aliasing effect. The worst case of SFDR is 38.3 dBc at the second-order harmonic frequency. The ghost-free dynamic range (GFDR) indicates the ratio between the input and smallest spuriousness, which is above the floor level and less than the harmonics and large spurious. These small spurious appear as $f_N/2 \pm f_R$ and $f_N - f_R$, where f_N is the Nyquist frequency and f_R is the input signal [26]. However, the expression of GDFR is not limited to this definition, and we will refer to small spurious groups collectively as GDFR in this study. GFDR occurs when acquiring the spectrum and is defined as 77.3 dBc in this device at 5.7 GHz. As shown in Fig. 3, GFDR is constant and independent of the frequency. These spurious signals also occur with 50-Ω termination and a 100-MHz clock input. The SFDRs are 16.2, 19.8, and 18.0 dB at 5.82, 6.16, and 6.49 GHz, respectively, and the GFDR is 1.25 dB at 5.66, 5.99, and 6.32 GHz. We have no problem with these current spurious, because these are distinguishable from true signal and can be removed by processing.

Fig. 4 presents the response of an input signal generated by a signal generator at 5.9 GHz. The relation between the input and output signals maintains linearity over a range of approximately 95 dB by varying the scale value during data acquisition. The dynamic range (DR) can be evaluated as follows [28]:

$$(\mathrm{DR}) = 20 \times \log_{10}\left(2^{\mathrm{bit}}\right). \tag{1}$$

This is consistent with the DR of the 16 bit being 96 dB. The linearity is satisfied if the input power ranges within the input frequencies. This DR covers the assumed signal strength input from the receiver to the FFT.

The performance of a spectrograph depends on the presence of spectral leakage and scallop loss, which is determined by the window function [29]. Spectral leakage is a phenomenon in which the power leaks to the side channels, which in turn reduces the spectrum peak compared to the true value. When a large power spectrum is observed, it hides the smaller peaks in the neighborhood and the spectrum of the frequency component that should not be included is observed. This is the problem of the leakage. The scalloping loss is a phenomenon in which the frequency spectrum deviates from a frequency channel with a lower peak than that of the matched channel. The scalloping loss leads to show up worse leakage as side effects. Fig. 5 shows the results obtained for spectral leakage and scalloping loss at approximately 5.9 GHz. The leakage of the neighboring channels of rectangular, Hanning, and Blackman windows are approximately −32.7, −6.01, and −4.50 dB, respectively. In contrast, the measurement results of the scalloping loss for frequencies shifted by half a frequency bin $f = 5.90715$ GHz from the fixed frequency channel $f = 5.90720$ GHz as the matching frequency are shown. The scalloping loss of the spectrometers is 1.1–3.9 dB. Spectral leakage and scallop loss are not significant issues because the linewidths of O_2 from an altitude of 10 km are on the scale of a few MHz from [1], and much wider than the channel separation.

By using a noise source and an amplifier, Allan variance measurement of MAHOS was conducted. In the test, a stabilized noise source was connected to the MAHOS input, and measurements were performed for an hour. The

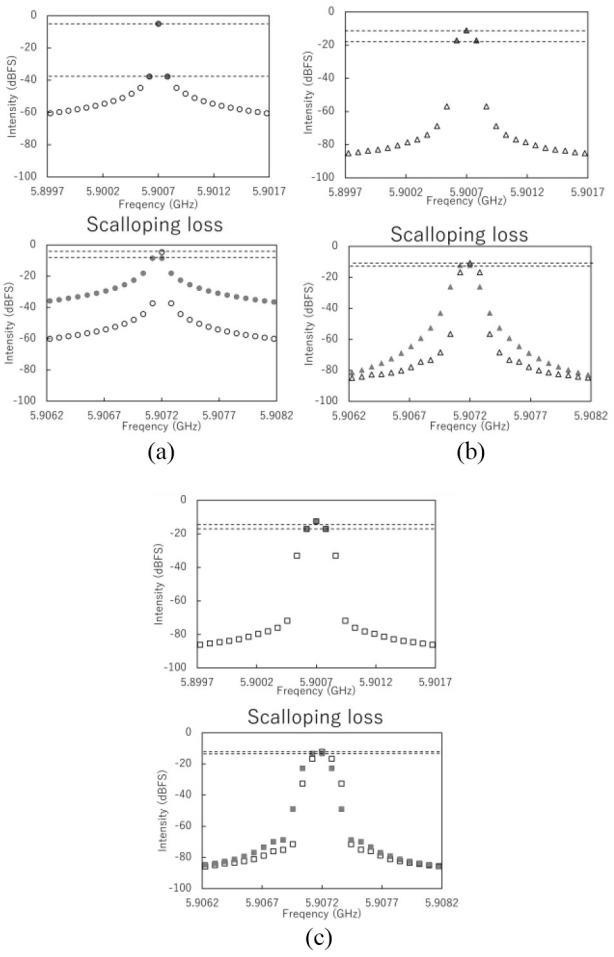

Fig. 5. Spectral leakage and scalloping loss around 5.9 GHz derived from (a) rectangular, (b) Hanning, and (c) Blackman window functions.

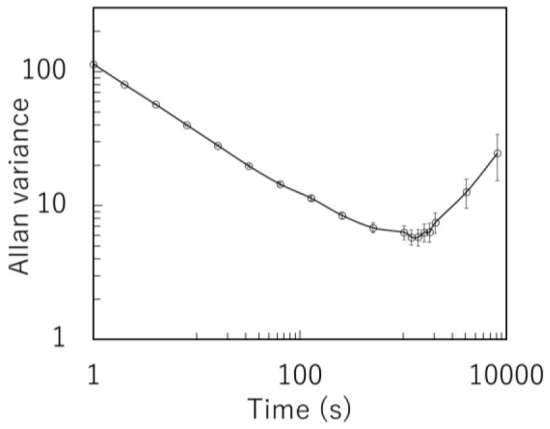

Fig. 6. Allan variance of FFT spectrometers at 5.8 GHz.

spectrometer, noise source, and amplifier were placed in a thermostatic chamber to ensure stability under room temperature. Fig. 6 shows the Allan variance plot for noise amplitude data acquired at 5.8 GHz. The result suggests that the signal averaging is in effect until around 1200 s at least. Since other frequency measurements over the 1-GHz band show similar results, MAHO is good stability for this time duration under the given environment condition.

TABLE III
MATERIAL PROPERTIES OF MAHOS

Material properties		Chassis	Accessories	PPE substrate
Mass (kg)		0.402	0.088	0.210
Modulus of Elasticity	MPa	69000	193000	14300
Poisson's ratio	-	0.3	0.3	0.2
Density ρ	kg/m^3	2700	7930	1820
allowable stress	MPa	275	-	-

B. Strength and Thermal Durability Analysis for Component Design

The vibration shock and thermal durability are important characteristics of the proposed spectrometer for space applications [30]. These simulation analyses confirm the static and dynamic behaviors, in response to the mechanical shock and vibrations of H2A rocket launch and to a hypothetical mission: landing on a planet. Numerical simulations were performed with the FEMAP with the NX NAS-TRAN software package of the integrator of a strength evaluation tool (IOSET) (*Technosolver Corporation*). A mechanical structure was modeled with 6437 nodes and 7438 elements for the structural analysis and a thermal model was made with 13 048 nodes and 9263 elements for the thermal analysis.

The important material properties are in Table III for the mechanical simulation.

Structural Analysis: A microsatellite and its payloads experience various loads during their mission. The shock is specified to be 100 G's with a sine half-wave of approximately 10 ms for perpendicular to the mounting surface of the spectrometer. MAHOS is designed to attach to the mounting surface with four screws. The first mode resonance frequency of the proposed whole receiver structure, including the effect of the other subsystems, is 176.6 Hz. To avoid resonances between the whole receiver and payloads, the resonance frequencies of the spectrometer that are larger than the certain values of the primary mode in the whole receiver are required. Fig. 7 shows the first three resonance modes of the structural model. Table IV presents the natural frequencies of the first ten modes with an effective mass ratio, which shows translational motion direction (x, y, z) for (T_1, T_2, T_3) and rotational motion direction (x, y, z) for (R_1, R_2, R_3). The ratio represents the effective mass component affected by each mode, which has assigned a larger value to the major mode. In case of the first mode at 431.8 Hz, which is a sufficiently high frequency, the effective mass proportions of T_1 and R_2 are 73.7% and 91.3%, respectively. Other mode frequencies in all directions are negligible compared with the first mode. Based on the natural frequency analysis, the system confirms that the structure has sufficiently high stiffness and will survive during launch without any deformation.

Static Load Analysis: The static analysis was also performed to estimate the stresses induced by the static loading of the structures and components. Fig. 8 shows the deformation and MS distribution in the x-, y-, and z-directions at a quasistatic acceleration of 1 G.

The structure responds with a maximum deflection of 2.0×10^{-6} m, which is acceptable in terms of the static

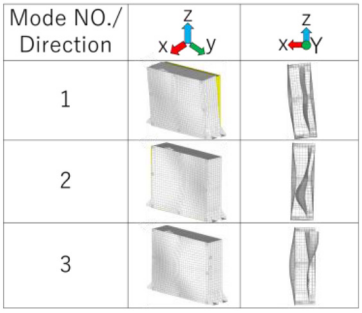

Fig. 7. First three modes of the structure.

TABLE IV
NATURAL FREQUENCIES OF THE FIRST TEN MODES WITH THE EFFECTIVE MASS RATIO

Modes	Characteristic vibration frequencies (Hz)	Effective mass ratio (%)					
		T_1	T_2	T_3	R_1	R_2	R_3
1	431.8	73.7	0.0	0.0	0.0	91.3	0.0
2	639.2	0.6	0.0	0.1	0.0	2.7	0.0
3	719.5	0.9	0.0	0.0	0.0	0.0	1.4
4	728.9	0.8	0.0	0.0	0.0	0.0	2.0
5	757.0	0.0	0.0	0.0	0.0	0.0	10.9
6	849.1	0.7	0.0	0.0	0.0	1.1	0.2
7	926.6	0.1	0.0	0.0	0.0	3.8	0.3
8	1049.1	0.1	0.0	0.1	0.0	0.0	0.1
9	1054.7	0.3	0.0	0.1	0.1	0.0	0.0
10	1073.6	0.1	0.1	5.7	1.0	0.3	0.0
-	Total	77.2	0.1	6.0	1.2	99.4	14.9

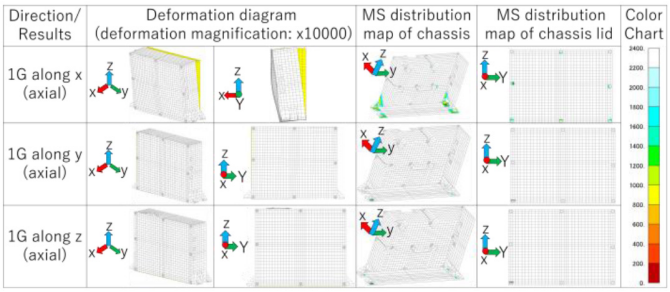

Fig. 8. Deformation and MS distribution under 1-G loading.

deflection interference of the other components. Fig. 8 also shows the margins of safety (MS) converted under the loading conditions equivalent to random vibration. MS indicates the margins of safety, and a negative MS indicates the occurrence of damage [31]

$$\text{MS} = \frac{(\text{Allowable applied load})}{(\text{Applied Load})} - 1. \tag{2}$$

In the x-direction, the structure experiences minimum stress of 303.2 at the legs. As the minimum MS at 1 G in the x-direction is 303.2, the allowable load is determined to be below $303.2 + 1 = 304.2$ G. Table V summarizes the minimum MS of the chassis and chassis lid [Fig. 2(a)].

Equivalent Loads Due to Random Vibration Analysis: Equipment can be subjected to random vibration, which can induce large stresses. The main purpose of performing this analysis is to confirm the resistance to a random vibration environment. This section presents the minimum MS

TABLE V
MINIMUM MS WITH 1 G ALONG EACH DIRECTION

Components	Minimum MS		
	1G along x-axis	1G along y-axis	1G along z-axis
Chassis	303.2	1600.1	1443.1
Chassis lid	799.0	2173.7	3226.1
Minimum value	303.2	1600.1	1443.1

TABLE VI
CONDITION OF RANDOM-VIBRATION EQUIVALENT LOAD

	1G along x-axis	1G along y-axis	1G along z-axis
$M_{3\sigma}$ (G)	160.1	323.5	252.5
minimum MS	0.9	3.9	4.7

at random vibration equivalent to the severe effective value set at 20 Grms. The static load analysis is performed at random-vibration equivalent load, assuming that the structure is subjected to launching loads of the H2A rocket. A load of structural strength is identified as the random vibration of the rocket according to the 3σ equivalent value (G_{RMS}) by using the following Miles' equation [32]:

$$M_{3\sigma} = 3 \times \sqrt{\frac{\pi}{2} \cdot Q \cdot f \cdot A_{psd}} \tag{3}$$

where Q is the response magnification, f is the resonant/natural frequency (Hz), and A_{psd} is the power spectral density at resonant frequency. The Q value is expressed using the following equation:

$$Q = \frac{1}{2\zeta\sqrt{1-\zeta^2}} \tag{4}$$

where ζ is the critical damping coefficient, which is sufficiently small; thus, the following equation holds in approximation:

$$Q = \frac{1}{2\zeta} = 20. \tag{5}$$

The condition of random-vibration equivalent load for each direction is calculated from the modal analysis results and this value. The minimum MS for the above load is calculated from the results obtained at 1 G. According to the result of the static load analysis and (3), the allowable yield stress and generated load for the x-axis are calculated as 304.2 and 160.11 G, respectively. As shown in Table VI, the MS of the random-vibration equivalent load is calculated as 0.9 for the x-direction, from (2). For the y- and z-axes, the MS can be calculated as 3.9 and 4.7, respectively. Therefore, in these cases, Miles's law for cumulative fatigue is implemented and the structure is found to have a large margin of safety.

Thermal Analysis: The thermal analysis can determine the heat damage caused by the effect on space instruments. The MAHOS installed on the microsatellite is subjected to a temperature of −15 to +50 °C during the operational conditions [9]. The heat conductivity (k) is the magnitude of a temperature gradient, which can be expressed as follows [33]:

$$k = \frac{t}{RA} \tag{6}$$

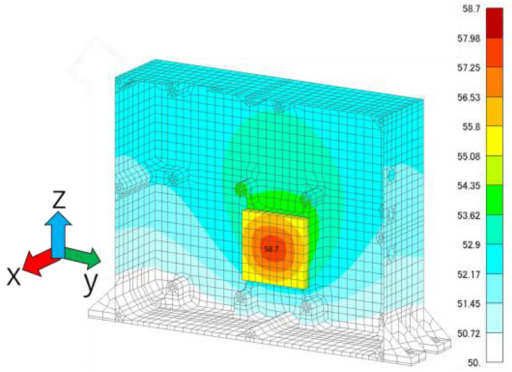

Fig. 9. Heat conduction analysis, without lid, substrate, and convex metal for thermal emission.

where $t(= 1.975 \times 10^{-3}$ m) indicates the thickness, $R(= 0.16\,°C/W)$ indicates the thermal resistance, and A $(= 0.035^2$ $m^2)$ indicates the heat transfer area. FPGA, as the only heat-generating component, is calculated as 10.08 W/m.°C. Based on the heat transfer coefficient of the material, thickness, several layers, and thickness and percentage of copper foil, the thermal conductivity of the substrate is determined as 52.4 W/m.K. The contact conditions include the material properties, the chassis and lid, the convex metal for thermal emission, and the substrate. With the outer surface at 50 °C considered the maximum hot condition, the FPGA junction in the enclosure is set to 7.1 W with two channels as a worst-case scenario. The output upper temperature limit for the junction is 63 °C. As shown in Fig. 9, the maximum temperature of the FPGA junction is 58.7 °C. Accordingly, the temperature will not exceed the upper junction temperature and the thermal damage will be avoided.

V. Conclusion

A compact and low-power-consumption MAHOS is developed as a THzSens component installed on a microsatellite. THzSens is a compact sensor that can simultaneously realize the observation of O_2 and H_2O concentrations at 480 GHz within 1-GHz bandwidth. This article presents the design and performance of MAHOS. The volume and weight of the spectrometer are approximately $0.154 \times 0.125 \times 0.040$ m^3 and 0.7 kg, respectively. The spectrometer comprises two channels as a redundant system. The advantage of MAHOS is the variable power consumption from 5 to 10 W due to the intermittent operation. In addition, the spectrometer has a high resolution, which is 2.6624 GS/s of the sampling speed with 16 384 frequency channels. Through the modal analysis, static load analysis, random vibration analysis, and thermal analysis, the design is demonstrated to be stiff and stable enough to survive during the launch. In addition, the structure has a large safety margin and does not resonate with the surrounding environment and does not deform during launch. In addition, the thermal damage can be avoided at a lower internal upper temperature limit.

Further tests of MAHOS will be conducted using other components of the THzSens receiver, thus revealing suitability under the total receiver conditions. For example, the stability of the spectrometer for space applications will be validated under temperature changes and the application of vibration shock. The entire backend from the horn to the data handling section will be confirmed to operate, and H_2O and O_2 peaks will be measured to verify the equivalent bandwidth and noise dynamic range.

Acknowledgment

The authors thankfully acknowledge the advice on the interface support provided by A. Uematsu and Y. Kakimi of the Japan Aerospace Exploration Agency. They would like to acknowledge K. Iwai for suggestions and advice regarding the method of spectrometer measurement. They also thank A. Mizuno at the Nagoya University and his team for telling them to provide information on a spectrometer. They also would like to thank Editage (www.editage.com) for English language editing.

References

[1] R. Larsson *et al.*, "Mars submillimeter sensor on microsatellite: Sensor feasibility study," *Geosci. Instrum. Methods Data Syst.*, vol. 7, no. 4, pp. 331–341, Dec. 2018.

[2] B. R. Sandel *et al.*, "Altitude profiles of O_2 on Mars from SPICAM stellar occultations," *Icarus*, vol. 252, pp. 154–160, May 2015.

[3] T. Fouchet *et al.*, "Martian water vapor: Mars Express PFS/LW observations," *Icarus*, vol. 190, no. 1, pp. 32–49, Sep. 2007.

[4] T. L. McDunn *et al.*, "Simulating the density and thermal structure of the middle atmosphere (∼ 80–130 km) of Mars using the MGCM–MTGCM: A comparison with MEX/SPICAM observations," *Icarus*, vol. 206, no. 1, pp. 5–17, Mar. 2010.

[5] P. Withers and R. Pratt, "An observational study of the response of the upper atmosphere of Mars to lower atmospheric dust storms," *Icarus*, vol. 225, no. 1, pp. 378–389, Jul. 2013.

[6] J. H. Booske *et al.*, "Vacuum electronic high power terahertz sources," *IEEE Trans. THz Sci. Technol.*, vol. 1, no. 1, pp. 54–75, Sep. 2011.

[7] Y. Kasai *et al.*, "Overview of the Martian atmospheric submillimetre sounder FIRE," *Planetary Space Sci.*, vols. 63–64, pp. 62–82, Apr. 2012.

[8] D. DePasquale and J. Bradford, *Nano/Microsatellite Market Assessment*, SpaceWorks Enterprises, Inc., Atlanta, CA, USA, Feb. 2013.

[9] R. Takahashi, R. Sakagami, A. Wachi, Y. Kasai, and S. Nakasuka, "The conceptual design of a novel, small and simple Mars lander," in *Proc. IEEE Aerosp. Conf.*, 2018, pp. 1–10.

[10] N. Kämpfer, *Monitoring Atmospheric Water Vapour*. New York, NY, USA: Springer, 2013, pp. 71–93. [Online]. Available: https://link.springer.com/book/10.1007/978-1-4614-3909-7

[11] L. Mazuray *et al.*, "SMILES/AOS: Acousto-optical spectrometer for high resolution submillimeter-wave spectroscopy," in *Proc. Sens. Syst. Next Gener. Satell. V*, vol. 4540. Toulouse, France, 2001, pp. 188–196. [Online]. Available: https://www.spiedigitallibrary.org/conference-proceedings-of-spie/4540/0000/SMILES-AOS–acousto-optic-spectrometer-for-high-resolution-submillimeter/10.1117/12.450660.short

[12] R. Schieder, J. Horn, O. Siebertz, M. Klumb, F. Frerick, and V. Tolls, "Acousto-optical spectrometers in space," in *Proc. ESTEC Conf.*, vol. 388. Noordwijk, The Netherlands, 1996, p. 187.

[13] V. Tolls *et al.*, "Submillimeter wave astronomy satellite performance on the ground and in orbit," *Astrophys. J. Suppl.*, vol. 152, no. 1, pp. 137–162, Jan. 2004.

[14] P. Hartogh, "High-resolution chirp transform spectrometer for middle atmospheric microwave sounding," in *Proc. Satell. Remote Sens. Clouds Atmosphere II*, vol. 3220. London, U.K., 1997, pp. 115–124. [Online]. Available: https://www.spiedigitallibrary.org/conference-proceedings-of-spie/3220/0000/High-resolution-chirp-transform-spectrometer-for-middle-atmospheric-microwave-sounding/10.1117/12.301141.short

[15] K. R. Skup *et al.*, "Design of DPU and PSU for ESA JUICE submillimeter wave instrument (SWI)," in *Proc. Photon. Appl. Astron., Commun., Ind. High Energy Phys. Exp.*, vol. 11176. Wilga, Poland, 2019, pp. 1063–1071. [Online]. Available: http://koral.ise.pw.edu.pl/ rrom/SPIE/SPIE11176-Wilga2019/art/111763K.pdf

[16] S. Polak *et al.*, "Design of the radiator for detection part of the submillimeter wave instrument (SWI) of JUICE mission," in *Proc. Photon. Appl. Astron. Commun. Ind. High Energy Phys. Exp.*, vol. 11176. Wilga, Poland, 2019, pp. 1147–1157. [Online]. Available: http://koral.ise.pw.edu.pl/ rrom/SPIE/SPIE11176-Wilga2019/art/111763U.pdf
[17] P. Hartogh *et al.*, "The submillimetre wave instrument on JUICE," in *Proc. Eur. Planetary Sci. Congr.*, London, U.K., 2013, Art. no. EPSC2013-710.
[18] A. Murk and K. Mikko, "Characterization of digital real-time spectrometers for radio astronomy and atmospheric remote sensing," in *Proc. 30th Int. Symp. Space THz Technol.*, vol. 15. Gothenburg, Sweden, 2019, pp. 139–142.
[19] C. Müller, A. Murk, C. Monstein, and N. Kämpfer, "Intercomparison of digital fast Fourier transform and accousto optical spectrometers for microwave radiometry of the atmosphere," *IEEE Trans. Geosci. Remote Sens.*, vol. 47, no. 7, pp. 2233–2239, Aug. 2009.
[20] B. Klein, S. D. Philipp, I. Krämer, C. Kasemann, R. Güsten and K. M. Menten "The APEX digital fast Fourier transform spectrometer," *Astron. Astrophys.*, vol. 454, no. 2, pp. L29–L32, Aug. 2006.
[21] *Fast Fourier Transform Spectrometer RPG_XFFTS Manual_2015*, Rohde & Schwarz Company, Radiometer Physics GmbH, Meckenheim, Germany, 2015. [Online]. Available: https://www.radiometer-physics.de/download/XFFTS/XFFTS%20Manual_2015.pdf
[22] B. Klein *et al.*, "The next generation of fast Fourier transform spectrometer," in *Proc. 19th ISSTT*, 2008, pp. 192–195.
[23] S. Heyminck, U. U. Graf, R. Güsten, J. Stutzki, H. W. Hübers, and P. Hartogh, "GREAT: The SOFIA high-frequency heterodyne instrument," *Astron. Astrophys.*, vol. 542, pp. L1–L8, Jun. 2012.
[24] Z. Yan, Y. Kim, A. Tang, J. Kawamura, R. Theodore, M.-C. F. Chang, "A 2.6 Gs/s spectrometer system in 65nm CMOS for spaceborne telescopic sensing," in *Proc. IEEE Int. Symp. Circuits Syst.*, Firenze, Italia, 2018, pp. 1–4.
[25] (2017). *A Compact Adaptable Microwave Limb Sounder for Atmospheric Composition (CAMLS)*. [Online]. Available: https://techport.nasa.gov/view/15873
[26] K. Iwai *et al.*, "OCTAD-S: Digital fast Fourier transform spectrometers by FPGA," *Earth Planets Space*, vol. 69, no. 1, pp. 1–8, Jul. 2017.
[27] M. Nakagawa *et al.*, "Compact 480 GHz radiometer calibration unit with specular-reflection absorber for atmospheric remote sensor onboard microsatellite," *IEEE Trans. THz Sci. Technol.*, early access, Jul. 7, 2021, doi: 10.1109/TTHZ.2021.3095436. [Online]. Available: https://ieeexplore.ieee.org/document/9477169
[28] A. Estrada, "Improving high speed analog to digital converter dynamic range by noise injection," in *Proc. IEEE Autotestcon*, 2007, pp. 669–676.
[29] R. Inkol and S. Wang, "A comparative study of FFT-summation and polyphase-FFT CFAR detectors," in *Proc. Can. Conf. Elect. Comput. Eng.*, vol. 2, 2004, pp. 1175–1178.
[30] A. Israr, "Vibration and modal analysis of low earth orbit satellite," *Shock Vib.*, vol. 2014, Jun. 2014, Art. no. 740102, doi: 10.1155/2014/740102.
[31] R. A. Beaulieu, *Margin of Safety Definition and Examples Used in Safety Basis Documents and the USQ Process*, Nevada Test Site/Nat. Security Technol., North Las Vegas, LV USA, 2013.
[32] R. Sahu, A. Hemant, and B. S. Munjal, "Semikinematic mount for spatially constrained high aspect ratio spacecraft fold mirrors," *Opt. Eng.*, vol. 56, no. 12, Dec. 2017, Art. no. 125101.
[33] F. Kreith, and W. Z. Black, *Basic Heat Transfer*. Manhattan, NY, USA: Harper and Row, 1980.

Maho Nakagawa received the Ph.D. degree in science from Nagoya University, Nagoya, Japan, in 2017.

From 2017 to 2018, she was involved in experimental and development observation instrument with an organic aerosol reactivity of ambient air in atmospheric chemistry as a Program-Specific Researcher and an Assistant Professor. Since 2019, this experience led to her work as a Project Scientist with the National Institute of Communication and Technology, Tokyo, Japan, where she has been involved with a submillimeter-wave components and experimental study of atmospheric remote sensing instruments. Her current research interests include submillimeter-wave receiver development and high-frequency measurement.

Dr. Nakagawa is a member of the Japan Society of Atmospheric Chemistry and the Japan Association of Aerosol Sciences and Technology.

Takayoshi Yamada received the Ph.D. degree in science from the Tokyo Institute of Technology, Tokyo, Japan, in 2018 for developing a submillimeter radiative transfer simulator, including rotational non-LTE model and data analysis of remote sensing.

He is a Researcher with the National Institute of Information and Communications Technology, Tokyo. His scientific research interests are terahertz radiative transfer modeling and remote sensing for Earth's and planetary atmosphere.

Shigeru Sato received the M.S. degree in condensed matter physics from Tokyo Metropolitan University, Hachioji, Japan, in 1977.

From 1977 to 1985, he was a Research Engineer with Konishiroku Photo Industry Company, Ltd. (Konica Minolta), Tokyo, Japan. He worked with Schlumberger K.K., Sagamihara, Japan, from 1985 to 2017 to develop measurement instruments for geophysical exploration used in oil wells. He is currently engaged in the development of a terahertz measurement unit for microsatellites with the National Institute of Information and Communications Technology, Tokyo. His current interests include measurement algorithms using stochastic estimation theory.

Ichiro Kato received the B.E. and M.E. degrees in physical engineering and the D.E. degree in electrical and electronic engineering from the University of Tokyo, Tokyo, Japan, in 1977, 1979, and 1997, respectively.

His M.E. theme was in relations to the exciton in magnetic semiconductors. He was a Researcher of Silicon MOSFET and related materials with Fujitsu Laboratories Ltd., Kanagawa, Japan, from 1979 to 1988. In 1997, he was with Fujitsu Ltd., Tokyo. He was an Invited Researcher for MEMS devices with JAXA, Tokyo, from 2011 to 2014. From 2016 to 2020, he was a URA with the Institute of Medical Science, University of Tokyo. He is currently engaged in the assistance of terahertz receiver development with the National Institute of Information and Communications Technology, Tokyo. His recent scientific interest is in optical quantum mechanics inside a living body.

Toshiyuki Nishibori received the B.E. degree in instruments and control engineering from Hosei University, Tokyo, Japan, in 1987, and the M.E. and D.E. degrees in electrical and electronics engineering from Sophia University, Tokyo, in 1992 and 1995, respectively.

From 1987 to 1992, he was with Ishikawajima Harima Heavy Industries Company, Ltd., Tokyo. From 1995 to 1998, he was a Lecturer with the Tokyo Metropolitan College of Aeronautical Engineering, Tokyo. He has been an Associate Researcher with the Institute of Space and Astronautical Science and engaged in the development of a time correction ground processing system for the Space Very Long Baseline Interferometry. In 1998, he joined the National Space Development Agency, where he is currently involved in the research and development of the Superconducting Submillimeter-Wave Limb-Emission Sounder to be aboard the Japanese Experiment Module of the International Space Station for observing stratospheric minor constituents related to ozone depletion. Since 2015, he has been the Senior Researcher of the Sensor System Research Group, Research and Development Directorate, Japan Aerospace Exploration Agency, Tsukuba, Japan. His current research interests include antenna design and measurements at frequency submillimeter-wave region, quasioptics, radar remote sensing, and ground penetrating radar.

Dr. Nishibori is a member of the Japan Society for Aeronautical and Space Sciences and the Astronomical Society of Japan.

Kenichi Harada received the B.S. degree in physics from the Tokyo University of Science, Tokyo, Japan, in 1996.

He is a Sales Engineer and an Engineering Manager with Elecs Industry Company, Ltd., Kanagawa, Japan. He was a Development Team Manager of the MAHOS at Elecs Industry.

Toru Taniguchi received the B.S. and M.S. degrees in physics from Kagoshima University, Kagoshima, Japan, in 2007 and 2009, respectively.

He is currently an Engineer with Elecs Industry Company, Ltd., Kanagawa, Japan. He was involved in the printed circuit board design and tests of the MAHOS at Elecs Industry.

Hiroaki Kawamoto received the B.S. degree in physics from Tokyo Metropolitan University, Tokyo, Japan, in 2018.

He is currently an Engineer with Elecs Industry Company, Ltd., Kanagawa, Japan. He was responsible for the FPGA design of the MAHOS at Elecs Industry.

Kazuyuki Nakamura received the master's degree in mechanical engineering from Yokohama National University, Yokohama, Japan, in 1986.

He worked on several Japanese satellite projects with Toshiba Corporation, Tokyo, Japan, from 1986 to 2001 and Mitsubishi Electric Corporation, Tokyo, from 2001 to 2003. In 2004, he established Technosolver Corporation, Kanagawa, Japan, which has the main business areas of consulting of structural analysis and space structures. His main areas of interest are structural analyses, satellite structures, and lightweight deployable structures for space application.

Mr. Nakamura is a member of the Japan Society of Mechanical Engineers, the Japan Society for Aeronautical and Space Sciences, and the American Institute of Aeronautics and Astronautics.

Takahiro Kuhara received the master's degree in engineering physics from Embry–Riddle Aeronautical University, Daytona Beach, FL, USA, in 2011.

He worked for the Uniform and Hodoyoshi projects from 2011 to 2013 with NESTRA, Kanagawa, Japan. He was in charged of the structure of three nanosatellites. Since 2013, he has been working with Technosolver Corporation, Kanagawa, Japan. His interests are spacecraft structure analysis and developments.

Yasuko Kasai received the Ph.D. degree from the Chemistry Department, Tokyo Institute of Technology, Tokyo, Japan, in 1995, with microwave molecular spectroscopy and radio astronomical observations.

She is an Executive Researcher with the National Institute of Information and Communications Technology, Tokyo, and also with the Physics Program, Graduate School of Pure and Applied Sciences, Tsukuba University. Her scientific research interests are on satellite remote sensing for Earth's and planetary atmosphere.